Tuning from failed superconductor to failed insulator with magnetic field

Yangmu Li,¹ J. Terzic,² P. G. Baity,², Dragana Popović,² G. D. Gu,¹ Qiang Li,¹ A. M. Tsvelik,¹, J. M. Tranquada^{1*}

¹Condensed Matter Physics and Materials Science Division,
Brookhaven National Laboratory, Upton, New York 11973, USA

²National High Magnetic Field Laboratory,
Florida State University, Tallahassee, Florida 32310, USA

*To whom correspondence should be addressed; E-mail: jtran@bnl.gov.

Do charge modulations compete with electron pairing in high-temperature copper-oxide superconductors? We investigated this question by suppressing superconductivity in a stripe-ordered cuprate compound at low temperature with high magnetic fields. With increasing field, loss of three-dimensional superconducting order is followed by reentrant two-dimensional superconductivity and then an ultra-quantum metal phase. Circumstantial evidence suggests that the latter state is bosonic and associated with the charge stripes. These results provide experimental support to the theoretical perspective that local segregation of doped holes and antiferromagnetic spin correlations underlies the electron-pairing mechanism in cuprates.

INTRODUCTION

A variety of electronic orders have been proposed and/or observed to exist within the generic phase diagram of copper-oxide high-temperature superconductors (1), and most are commonly viewed as competing with the superconducting order. In the case of charge-stripe order (2), however, it has been argued that electron pairing and superconducting order can actually be intertwined with the charge modulations (3). Moreover, increasingly powerful numerical calculations indicate that charge stripes are a natural consequence of doping holes into a correlated antiferromagnetic insulator (4,5) and can exhibit superconducting correlations (6,7). While charge stripe order is readily observed within the CuO₂ planes of compounds such as La_{2-x}Ba_xCuO₄ (LBCO) (8), experimentally establishing a positive connection with superconductivity has been challenging. One theoretical expectation for a superconductor based on stripes is that the magnitude of the energy gap associated with pair correlations within charge stripes should be much greater than the energy associated with coherent coupling between the stripes (9), and here we test the implications of this picture. We use a transverse magnetic field first to decouple the superconducting planes in LBCO with x = 0.125 and then to destroy the superconducting order within the planes. We discover an ultra-quantum metal phase that we argue cannot be explained by conventional fermionic quasiparticles, in sharp contrast to the high-field behavior in YBa₂Cu₃O_{6+x} at a similar hole concentration (10). We conclude that it provides circumstantial evidence that charge stripes can exhibit robust pairing correlations.

What is already known about LBCO? The spin and charge stripe orders have been previously studied by neutron and x-ray diffraction techniques in magnetic fields perpendicular to the CuO_2 planes up to approximately 10 T. For hole concentrations close to x = 0.125, the field enhances the stripe order parameters (11), while right at x = 0.125 it simply increases the charge-stripe correlation length (12). [Field-induced charge order has been reported in YBa₂Cu₃O_{6+x} in fields up to 28 T (13).] While the bulk T_c is suppressed to ~ 5 K in zero field

for x=0.125, a substantial decrease in the ab-plane resistivity already occurs below ~ 40 K, with additional evidence for a transition to two-dimensional (2D) superconducting order near 16 K (14). One would expect Josephson coupling between neighboring layers to induce 3D superconducting order as soon as 2D superconductivity develops; the apparent frustration of the interlayer Josephson coupling has been explained in terms of a proposed pair-density-wave (PDW) state, which involves a strong pairing amplitude on the 1D charge stripes but with opposite signs of the pair wave function on neighboring stripes (15, 16). In LBCO with x=0.095, where the 3D superconductivity is more robust, a magnetic field perpendicular to the CuO₂ planes causes a decoupling into 2D superconducting layers (17).

RESULTS

Following the first successful growth of a $\text{La}_{2-x}\text{Ba}_x\text{CuO}_4$ single crystal with $x \sim 1/8$ and observation of stripe order by neutron diffraction (18), one of the authors (G.D.G.) devoted considerable time to growing a series of large crystals with $0.095 \le x \le 0.155$ in steps of $\Delta x = 0.02$ utilizing infrared image furnaces and the traveling solvent floating-zone technique (19). X-ray and neutron diffraction studies have demonstrated that the structural transitions and lattice parameters are quite sensitive to x, providing valuable and reliable measures of stoichiometry (8). The crystals of x = 0.125 were originally grown for a neutron-scattering study of the spin dynamics (20), and have since been characterized by transport (14, 21) and optical conductivity (22). The crystals used in the present study, described further in the Materials and Methods section, were from the same growth.

A partial summary of our observations is presented in Fig. 1A as a color contour map of electrical resistivity as a function of temperature and magnetic field. The electrical resistivity is presented throughout this work in terms of the resistance per CuO_2 sheet (sheet resistance), $R_s = \rho_{ab}/d$, where d = 6.6 Å is the layer separation, with the magnitude in units of the quantum

of resistance for electron pairs, $R_Q = h/(4e^2) = 6.45 \text{ k}\Omega$, where h is Planck's constant and e is the electron charge. An increase of R_s through R_Q is associated with the localization of electron pairs, as observed in the carrier-density-tuned superconductor-insulator transition for La₂ $_{-x}\text{Sr}_x\text{CuO}_4$ thin films (23). At low temperatures with increasing magnetic field H, we observe a progression from 3D superconducting order, through a reentrant 2D superconducting order, to an anomalous high-field metallic state with a sheet resistance saturated at $R_s \approx 2R_Q$. We denote this unanticipated state as an ultra-quantum metal (UQM): it is a metal because the resistance appears not to change as the temperature is reduced towards zero, and it is "ultra-quantum" because the magnitude of R_s cannot be explained by the usual semiclassical models. Another significant observation is that the Hall coefficient R_H is negligible below 15 K for the full field range (see Fig. 1B and Fig. S2 in the SM), a behavior expected in a superfluid of bosonic Cooper pairs, but that survives even in the UQM phase.

Before proceeding to the high-field results, we first consider the temperature dependence of R_s in zero-field. It is known from previous work that the anisotropy between the c-axis resistivity, ρ_c , and the in-plane resistivity, ρ_{ab} , is $\sim 10^4$ near 40 K, and rises to $\sim 10^5$ below the onset of 2D superconducting correlations (14). This large anisotropy makes the measurement of ρ_{ab} quite sensitive to sample imperfections. The inset of Fig. 2 shows the sample configuration; the current is directly injected into the CuO_2 planes and the voltage probes contact the edges of those same planes. If there is a slight misorientation of the crystal such that the c-axis is not precisely perpendicular to the current direction, then a small fraction of the current path will be along the c axis, making the measurement sensitive to ρ_c . With that preface, consider the measurements of R_s shown in Fig. 2 for two samples, A and B, with results from voltage contacts on both sides of A, labelled A1 and A2. The responses observed for A1 and A2 are consistent with previous work (14): a slight jump in R_s and change in slope at 56 K, corresponding to a well-known structural transition and the coincident charge-stripe ordering (8, 18),

and a large decrease below ~ 36 K indicating the mean-field transition to 2D superconductivity. In contrast, sample B shows a distinct behavior, with a larger magnitude of R_s at high temperature, a significant enhancement of resistance on cooling, and a peak in resistivity at 29 K. Such behavior, which resembles that of ρ_c (14) and has been reproduced in other samples, indicates a contribution from ρ_c consistent with a misorientation of $\sim 1.5^\circ$. (See the SM for further details.) The differences between samples A and B, while unintended, provide valuable information regarding the field-dependent behavior.

Next we consider the magnetic-field dependence of R_s measured at various fixed temperatures. Data for A1, A2, and B up to 35 T are shown in Fig. 3A-C. At low temperature, we find that the data collapse with a simple $ad\ hoc$ scaling determined by characteristic fields H_{3D} and H_{2D} . We define H_{3D} to be the field at which we detect an initial onset of finite resistivity, indicating loss of 3D superconducting order. H_{2D} corresponds to the mid-range of the reentrant 2D superconductivity, as discussed below. (In practice, it was determined by the corresponding local maximum in R_s for A2.) Figure 3D-F show R_s plotted vs. $(H - H_{2D})/\Delta H$, where $\Delta H = H_{2D} - H_{3D}$. Here we see that all three data sets are identical up to H_{3D} . For A1, R_s then returns to zero for a finite range of field. In the same region, B shows a rise to above $4R_Q$, consistent with insulating behavior in the ρ_c contribution due to putative PDW order and 2D superconductivity (16, 17).

The surprising behavior occurs for A2, where R_s virtually plateaus at R_Q for $H \sim H_{\rm 2D}$; however, it is also a consistent response for a 2D superconductor in a strong magnetic field. The field penetrates the sample as magnetic flux quanta that are screened by vortices of superconducting current. If the vortices are pinned by a combination of quenched disorder and electromagnetic interactions between layers (17, 24), then R_s will be zero (as observed for A1); on the other hand, if the vortices are not pinned in one part of the sample, dissipation will be observed (as for A2). In a model for the field-driven superconductor-insulator transition in

disordered 2D superconductors, a boson-vortex duality has been proposed, which predicts that $R_s = R_Q$ when the vortices can flow freely, provided that $R_{\rm H} = 0$ (25, 26) as in the present case.

Of course, the quantized vortices are only defined when a locally-coherent supercurrent is present. A 2D superconductor can only be ordered in the limit of zero current (27); with a finite current, we weaken the superconducting correlations and introduce a finite resistance. To the extent that the boson-vortex duality applies, we may expect a complementary effect on the vortices. We demonstrate this complementarity in Fig. 4A and B. At T=5 K, R_s for A1 is already finite in the 2D superconducting regime, and we observe that it increases with the measurement current. In contrast, for A2, R_s decreases as the current is raised. This effect is also clearly demonstrated in Fig. 4C, which compares the current-dependent R_s for A1 and A2 at $H \approx H_{\rm 2D}$ and $T \approx 1$ K: here, the changes for A1 and A2 are essentially equal and opposite. A similar trend is demonstrated by a plot of R_s at $H \approx H_{\rm 2D}$ vs. temperature for A1 and A2, as in Fig. 4D.

The most remarkable feature is the ultra-quantum metal phase at high field. Looking at Fig. 3D and E, we see for A1 and A2 that the rising field eventually destroys the 2D superconducting correlations and causes a large rise in R_s , which then starts to saturate for $H > H_{\rm UQM}$. (In the figure, the scaling based on $H_{\rm 2D}$ and $H_{\rm 3D}$ also collapses the curves at the transition to the UQM phase, so we define $H_{\rm UQM} \equiv H_{\rm 2D} + \Delta H$.) From the scaling, it is clear that $R_s \to 2R_Q$ in the limit of $T \to 0$ when H is sufficiently above $H_{\rm UQM}$. Although the saturation limit is large, the fact that we approach saturation is consistent with a metallic state within the CuO₂ planes. This state is also unusual for a metal in that $R_H \approx 0$. We note that related results have been observed in a study of Eu-doped La_{2-x}Sr_xCuO₄ (28).

Sample B shows complementary behavior, with R_s decreasing substantially above H_{UQM} . Loss of the 2D superconducting order leads to a dramatic reduction in the magnitude of the ρ_c contribution to R_s for sample B. Based on the ρ_c contribution to B, we estimate that ρ_c/ρ_{ab} drops to $<10^2$ at T=3 K (details in SM), compared to 10^4 at zero field and T=40 K. We also note for sample B that R_s depends on the measurement current for $H>H_{\rm 2D}$, as shown in Fig. S5.

DISCUSSION

What do these results tell us about the UQM phase? The standard theoretical description of a metal is in terms of fermionic quasiparticles. To estimate the transport properties due to fermionic excitations at low temperature after suppression of superconductivity, we can extrapolate from the zero-field normal state response previously reported for T > 40 K (14, 21). In particular, ρ_c has a large, nonmetallic magnitude that grows with cooling, and extrapolates to insulating behavior. If we assume that quasiparticles could explain our observations for A1 and A2, we would then expect to have $\rho_c/\rho_{ab} > 10^4$, inconsistent with our results for B. Inplane quasiparticles should also yield a finite value of $R_{\rm H}$, as observed in YBa₂Cu₃O_{6+x} at high field (29), which is, again, contrary to our results for LBCO.

The Hall constant is zero in the superconducting state because of the particle-hole symmetry of the Bogoliubov quasiparticles that make up the Cooper pairs. The observation that $R_{\rm H}$ remains negligible at high field suggests that such symmetry may survive. Such behavior (zero Hall resistivity and finite longitudinal resistivity) has been observed previously in disordered 2D superconductors (30), and hence our observations are not entirely unique. Nevertheless, the longitudinal resistivity in that case is much smaller than in the normal state, corresponding to the recently discussed "anomalous metal regime" (31). Our situation is different, with an inplane metallic resistance much larger than in the normal state at, for example, T=50 K, and hence it requires a distinct interpretation.

It was noted quite some time ago that superconducting order in underdoped cuprates may

be limited by phase coherence and not by electron pairing (32). In the present case, we have destroyed the superconducting phase coherence with the magnetic field, but electron pairs may survive. It has also been proposed, in a model based on coupled charge stripes, that strong electron-pair correlations might live within the charge stripes, with pair hopping between stripes providing the phase coherence (9, 33). The large magnitude of R_s in the UQM state is consistent with localization of surviving electron pairs within charge stripes; nevertheless, incoherent tunneling of Bosonic pairs between stripes could yield finite conductivity (failed insulator). Regarding the c-axis response inferred from sample B, the large magnitude of R_s in the 2D regime is consistent with PDW order, which results in cancellation of interlayer pair tunneling (16, 34) (failed 3D superconductor); with the loss of that order, even limited tunneling of pairs between layers would reduce ρ_c/ρ_{ab} in the UQM phase, as appears to happen. The nonlinear transport in sample B (shown in the SM) is also suggestive of pairing correlations that can be destroyed by high current density.

The experimental results leave us with the implication that the UQM phase is a Bose metal. There have been various theoretical proposals of a Bose metal state, but applications to real materials have so far been confounded by coexisting fermionic quasiparticles (31). In LBCO at high field, quasiparticles do not appear to be relevant. While further experimental and theoretical work is needed, we believe that our circumstantial evidence supports the perspective that charge stripes in cuprates, including dynamic stripes, are good for electron pairing (5–7, 33, 35, 36), even if stripe ordering may limit the degree of superconducting phase coherence.

MATERIALS AND METHODS

Materials and sample preparation Several samples were oriented with Laue x-ray diffraction, cut from the large crystal with a wire saw, and polished with diamond sand paper down

to 0.3- μ m roughness, achieving an almost perfect rectangular shape for direct ab-plane charge transport measurements. No defects or cracks were visible on the surfaces of the samples. PELCO and Dupont 6838 silver paste and gold wires were used to contact samples in a Hall bar geometry, and samples were annealed in air flow at 450 degrees Celsius to minimize the contact resistance. The current contacts were made by covering the whole area of the two opposing ends to ensure uniform current flow, and the voltage contacts were made narrow to minimize the uncertainty in the absolute values of the resistance (inset of Fig. 2a). Detailed high field measurements were performed on two samples, A and B, with dimensions $3.85 \times 0.94 \times 0.53$ mm³ and $3.08 \times 1.24 \times 0.58$ mm³ ($a \times b \times c$), respectively.

Charge transport measurements A standard four probe configuration was used for charge transport measurements. Zero-field resistivity was measured using a helium cryostat, Signal Recovery 7265 lock-in amplifiers, Keithley 6220 current sources, and Keithley 2182A nanovolt meters.

The measurements as a function of magnetic field were performed with the 35 Tesla resistive magnet and a helium-3 cryostat at the DC Field Facility, National High Magnetic Field Labo-ratory. A straight probe was used to measure two samples at the same time. Signal Recovery 7265 and Stanford Research 865A lock-in amplifiers, Keithley 2182A nanovolt meters, Lake Shore 372 ac resistance bridges, were used to measure magnetoresistivity and Hall coefficient. Magnetoresistivity measurements were done with low frequency ac current at 31.6 μ A for 0.35 K $\leq T < 5$ K and with currents of 31.6, 100, 316 μ A for 5 K $\leq T \leq$ 50 K. Distinct frequencies were used (13 Hz for sample A, 16 Hz for sample B) to avoid crosstalk. Hall measurements were done with currents of 31.6 μ A for T < 25 K and 100 μ A for $T \geq 25$ K to minimize heating effects at low temperatures and the noise level at high temperatures. All measurements were performed by fixing the temperature and sweeping the field, with the sweep rate varying

from 1 T/min at low temperatures to 3 T/min at high temperatures.

ac dV/dI measurements of nonlinear resistivity were performed with Signal Recovery 7265 and Stanford Research 865A lock-in amplifiers, Keithley 2182A nanovolt meters, and DL Instruments 1211 current preamplifers, with an instrumentation set-up similar to that used in a previous work (23). ac voltage across the sample was measured by applying a dc current bias $(10-200~\mu\text{A})$, provided by Keithly 6221 current sources) and a small ac current excitation ($\sim 10~\mu\text{A})$) at 13 and 16 Hz. Joule heating was negligible at high temperatures (Fig. 4) and relatively small compared to nonlinear resistivity signals at low temperatures. dV/dI measurements were performed at $0.4~\text{K} \leq T \leq 5~\text{K}$.

Supplementary materials

Estimation of c-axis misorientation for sample B.

- Fig. S1. Temperature-magnetic field phase diagram for A2.
- Fig. S2. Field-dependence of Hall voltage at various temperatures.
- Fig. S3. Sheet resistance at constant magnetic field.
- Fig. S4. ac nonlinear resistivity at H2D for various temperatures.
- Fig. S5. Additional results for sample B.
- Fig. S6. Comparison between A1 and previous results for a similar sample.

References

- 1. B. Keimer, S. A. Kivelson, M. R. Norman, S. Uchida, J. Zaanen, *Nature* **518**, 179 (2015).
- 2. J. Orenstein, A. J. Millis, *Science* **288**, 468 (2000).
- 3. E. Fradkin, S. A. Kivelson, J. M. Tranquada, Rev. Mod. Phys. 87, 457 (2015).
- 4. B.-X. Zheng, et al., Science **358**, 1155 (2017).

- 5. E. W. Huang, et al., Science 358, 1161 (2017).
- 6. S. R. White, D. J. Scalapino, *Phys. Rev. B* **79**, 220504 (2009).
- 7. P. Corboz, T. M. Rice, M. Troyer, *Phys. Rev. Lett.* **113**, 046402 (2014).
- 8. M. Hücker, et al., Phys. Rev. B 83, 104506 (2011).
- 9. E. W. Carlson, D. Orgad, S. A. Kivelson, V. J. Emery, *Phys. Rev. B* **62**, 3422 (2000).
- 10. S. E. Sebastian, C. Proust, Annu. Rev. Condens. Matter Phys. 6, 411 (2015).
- 11. M. Hücker, et al., Phys. Rev. B 87, 014501 (2013).
- 12. J. Kim, A. Kagedan, G. D. Gu, C. S. Nelson, Y.-J. Kim, *Phys. Rev. B* 77, 180513 (2008).
- 13. S. Gerber, et al., Science **350**, 949 (2015).
- Q. Li, M. Hücker, G. D. Gu, A. M. Tsvelik, J. M. Tranquada, *Phys. Rev. Lett.* 99, 067001 (2007).
- 15. A. Himeda, T. Kato, M. Ogata, *Phys. Rev. Lett.* **88**, 117001 (2002).
- 16. E. Berg, et al., Phys. Rev. Lett. 99, 127003 (2007).
- 17. Z. Stegen, et al., Phys. Rev. B 87, 064509 (2013).
- 18. M. Fujita, H. Goka, K. Yamada, J. M. Tranquada, L. P. Regnault, *Phys. Rev. B* **70**, 104517 (2004).
- 19. H. Tanabe, S. Watauchi, I. Tanaka, H. Kojima, *Advances in Superconductivity X*, K. Osamura, I. Hirabayashi, eds. (Springer, Tokyo, 1998), p. 371.
- 20. J. M. Tranquada, et al., Nature **429**, 534 (2004).

- 21. J. M. Tranquada, et al., Phys. Rev. B 78, 174529 (2008).
- 22. C. C. Homes, et al., Phys. Rev. B 85, 134510 (2012).
- 23. A. T. Bollinger, et al., Nature 472, 458 (2011).
- 24. K. S. Raman, V. Oganesyan, S. L. Sondhi, *Phys. Rev. B* **79**, 174528 (2009).
- 25. M. P. A. Fisher, *Phys. Rev. Lett.* **65**, 923 (1990).
- N. P. Breznay, M. A. Steiner, S. A. Kivelson, A. Kapitulnik, *Proc. Natl. Acad. Sci. USA* 113, 280 (2016).
- 27. D. S. Fisher, M. P. A. Fisher, D. A. Huse, *Phys. Rev. B* **43**, 130 (1991).
- 28. Z. Shi, P. G. Baity, T. Sasagawa, D. Popović, Unveiling the phase diagram of a striped cuprate at high magnetic fields: Hidden order of Cooper pairs, https://arxiv.org/abs/1801.06903 (2018).
- 29. D. LeBoeuf, et al., Nature **450**, 533 (2007).
- 30. N. P. Breznay, A. Kapitulnik, Sci. Adv. 3 (2017).
- 31. A. Kapitulnik, S. A. Kivelson, B. Spivak, Rev. Mod. Phys. 91, 011002 (2019).
- 32. V. J. Emery, S. A. Kivelson, *Nature* **374**, 434 (1995).
- 33. V. J. Emery, S. A. Kivelson, O. Zachar, *Phys. Rev. B* **56**, 6120 (1997).
- 34. S. Rajasekaran, et al., Science 359, 575 (2018).
- 35. J. Zaanen, O. Y. Osman, H. V. Kruis, Z. Nussinov, J. Tworzydło, *Phil. Mag. B* **81**, 1485 (2001).
- 36. S. T. Carr, A. M. Tsvelik, *Phys. Rev. B* **65**, 195121 (2002).

Acknowledgments: The authors are grateful to E. S. Choi and S. Maier for assistance with the experiment, and to E. Berg, M. S. Foster, E. Fradkin, S. A. Kivelson, and A. Sapkota for valuable discussions and comments. Funding: Work at Brookhaven is supported by the Office of Basic Energy Sciences, Materials Sciences and Engineering Division, U.S. Department of Energy (DOE) under Contract No. DE-SC0012704. The work at National High Magnetic Field Laboratory and Florida State University was supported by NSF Grants No. DMR-1707785. A portion of this work was performed at the National High Magnetic Field Laboratory, which is supported by National Science Foundation Cooperative Agreement No. DMR-1644779 and the State of Florida. Author contributions: J.M.T., Q.L., and D.P. conceived the experiment. G.D.G. grew the crystals. Y.L., J.T., and P.G.B. performed the experiments. Y.L., D.P, A.M.T., and J.M.T. wrote the paper, with input from all authors. Competing interests: The authors declare that they have no competing interests. Data and materials availability: All data needed to evaluate the conclusions in the paper are present in the paper and/or the Supplementary Materials. Additional data available from authors upon request.

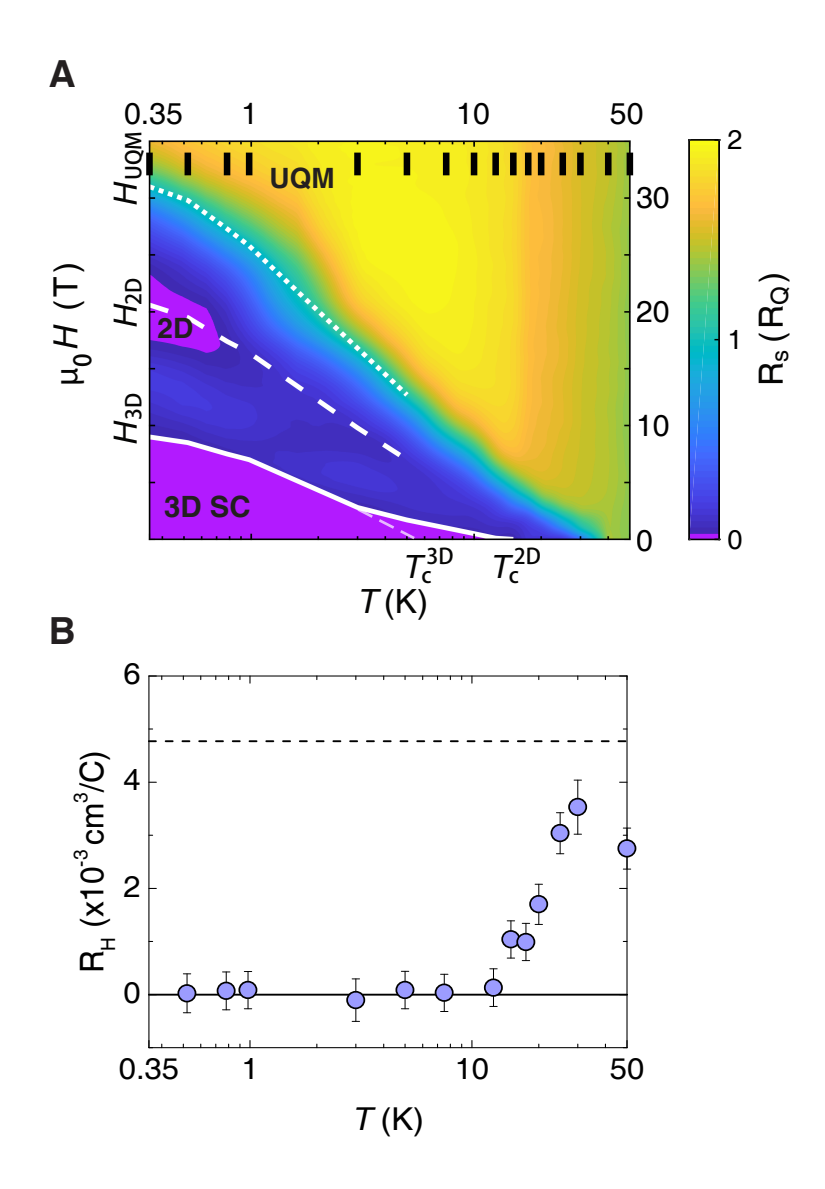


Figure 1: **Phase diagram of La**_{2-x}**Ba**_x**CuO**₄ with x=0.125 in terms of sheet resistance and Hall coefficient. (A) Interpolated color contour plot of the sheet resistance R_s as a function of temperature and magnetic field. Black vertical marks indicate measurement temperatures. The regimes of 3D and 2D superconductivity with zero electrical resistance are labeled; the ultraquantum metal phase occurs at fields above the dotted line. Characteristic fields H_{3D} , H_{2D} , and H_{UQM} (defined in the text) are over-plotted as solid, dashed, and dotted white lines, respectively. (These results are for sample A1; for an analogous plot for sample A2, see Fig. S1.) (B) Hall coefficient as a function of temperature, with error bars obtained by averaging over the entire field range (0 to 35 T, see Fig. S2) at each temperature. $R_{\rm H}$ is effectively zero below 15 K, as expected for a superconductor, and it rises to the normal-state magnitude around ~ 40 K. The upper dashed line indicates the magnitude of R_H that would be expected in a one-band system with a nominal hole density of 0.125. Results from sample A, as described in the text.

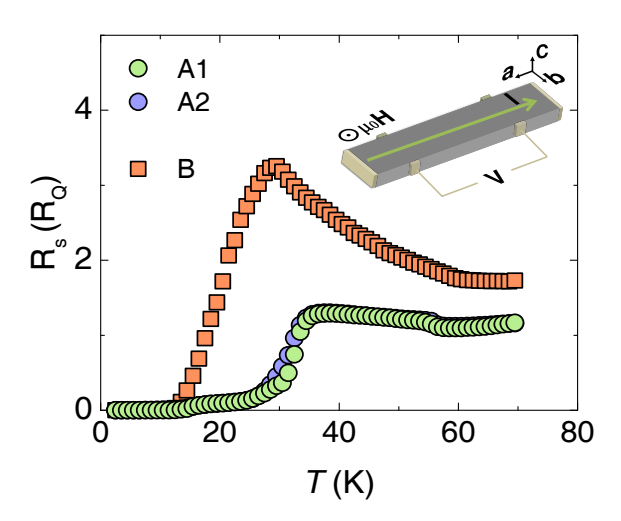


Figure 2: Sheet resistance in zero magnetic field. R_s as a function of temperature for samples A (circles) and B (squares). Inset shows sample and standard four-probe measurement configuration. Sample A has voltage contacts on two edges, resulting in measurements labelled A1 and A2. The difference between samples A and B is consistent with a small c-axis contribution to the resistance of B due to a slight misorientation of the c axis.

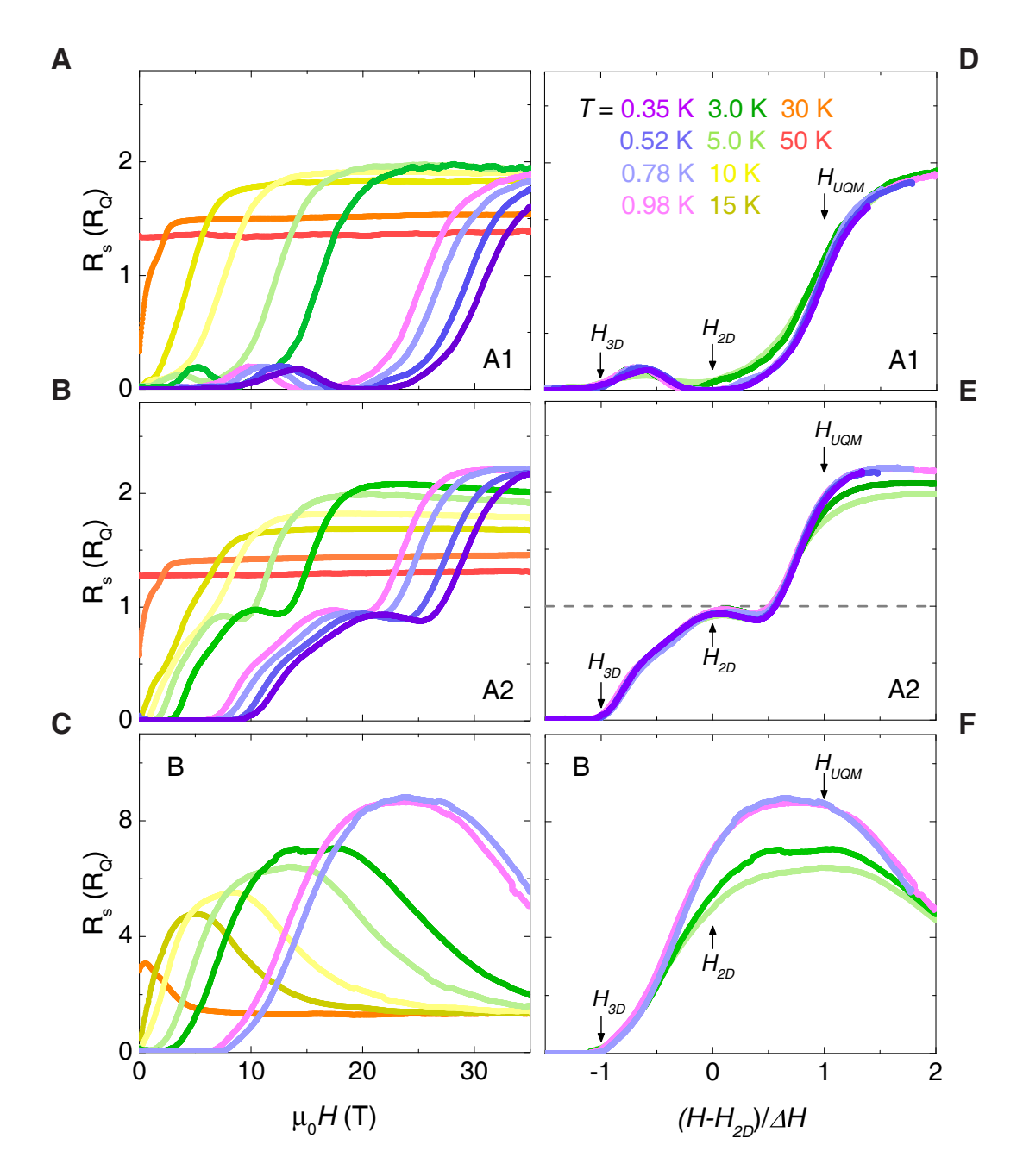


Figure 3: Sheet resistance as a function of magnetic field. Results at various temperatures for samples (A) A1, (B) A2, and (C) B. (D)-(F) show the same data plotted vs a scaled magnetic field, as discussed in the text. $H_{\rm 2D}$ corresponds to the field at which zero resistance is seen in A1 and a local maximum of $R_s \approx R_Q$ occurs in A2. Measurement temperatures are color coded, as indicated in (D). R_s was measured with an ac current of 31.6 μ A. (For plots of R_s vs. T, see Fig. S3.)

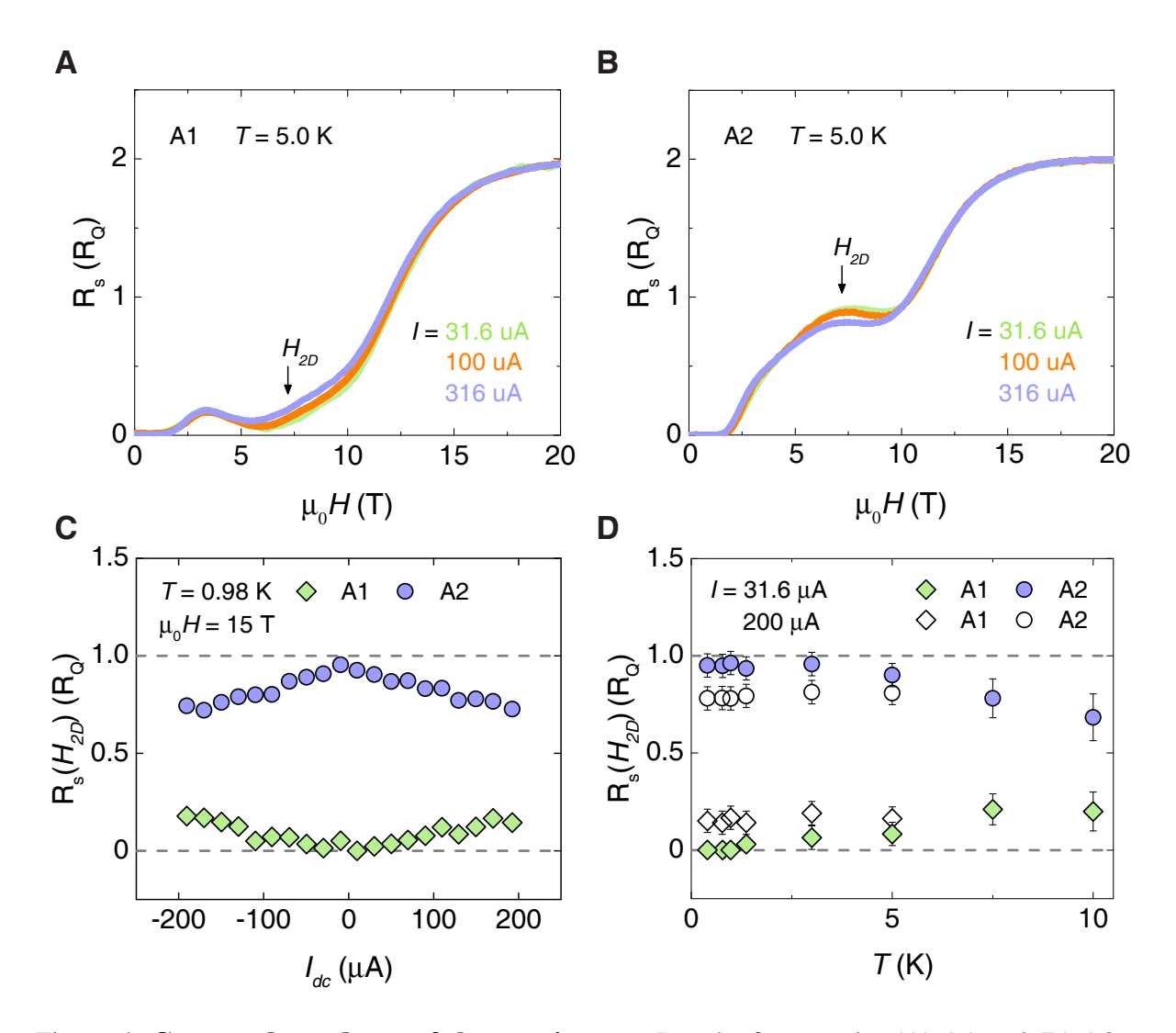


Figure 4: Current dependence of sheet resistance. Results for samples (A) A1 and (B) A2 at $T=5.0~\rm K$ with various currents. A significant difference between measurements is observed only in the 2D SC regime. (C) Current dependence of sheet resistance at $\mu_0H=15~\rm T\approx H_{\rm 2D}$ at $T=0.98~\rm K$ for samples A1 (diamonds) and A2 (circles), obtained by nonlinear dV/dI measurements with an ac current of $\sim 10~\mu \rm A$, in addition to the larger dc current (see Materials and Methods). (D) Variation of sheet resistance at $H\approx H_{\rm 2D}$ as a function of temperature measured with dc currents of 31.6 (filled symbols) and 200 $\mu \rm A$ (open symbols). (Further data are presented in Fig. S4.)



Supplementary Materials for

Tuning from failed superconductor to failed insulator with magnetic field

Yangmu Li, J. Terzic, P. G. Baity, Dragana Popović, G. D. Gu, Qiang Li, A. M. Tsvelik, J. M. Tranquada

Correspondence to: jtran@bnl.gov

This PDF file includes:

Estimation of c-axis misorientation for sample B

- Fig. S1. Temperature-magnetic field phase diagram for A2.
- Fig. S2. Field-dependence of Hall voltage at various temperatures.
- Fig. S3. Sheet resistance at constant magnetic field.
- Fig. S4. ac nonlinear resistivity at H_{2D} for various temperatures.
- Fig. S5. Additional results for sample B.
- Fig. S6. Comparison between A1 and previous results for a similar sample.

Estimation of c-axis misorientation for sample B

The *c*-axis misorientation in sample B can be estimated based on the zero-field resistivities of samples A and B, and the previous measurement of ρ_c in Ref. 14, all at T=40 K. We have $\rho_A=0.5$ m Ω cm $\approx \rho_{ab}$, $\rho_B=1.05$ m Ω cm, and $\rho_c=800$ m Ω cm. Solving Laplace's equation for the anisotropic resistivity tensor assuming a small misalignment angle α , we obtain:

 $\rho_{\rm B} = \rho_{ab} \cos^2 \alpha + \rho_c \sin^2 \alpha \approx \rho_{ab} + \rho_c \alpha^2.$

Hence, we find that $\alpha = \sqrt{(\rho_B - \rho_A)/\rho_c} \approx 0.026$, which corresponds to 1.5°.

We can also invert the formula in order to estimate the resistivity anisotropy at high field. We find: $\rho_c/\rho_{ab} \approx [(\rho_B/\rho_A) - 1]/\alpha^2$. We are interested in the anisotropy ratio in the UQM state at 35 T. We have to pick a temperature where R_s of A1 is saturated, and take T = 3.0 K. Then from Fig. 3, we find that R_s values for A1 and B are 1.93 R_Q and 2.03 R_Q , respectively. This yields $\rho_c/\rho_{ab} \approx 77 < 10^2$. We note a 10 percent uncertainty in the measurement of sample dimensions. Taken this effect to its extreme, assuming $\rho_A = 0.9 \times 1.93 R_Q$ and $\rho_B = 1.1 \times 2.03 R_Q$, we obtain $\rho_c/\rho_{ab} \approx 391$, still much less than the nominal resistivity anisotropy $\sim 10^4$ at zero field.

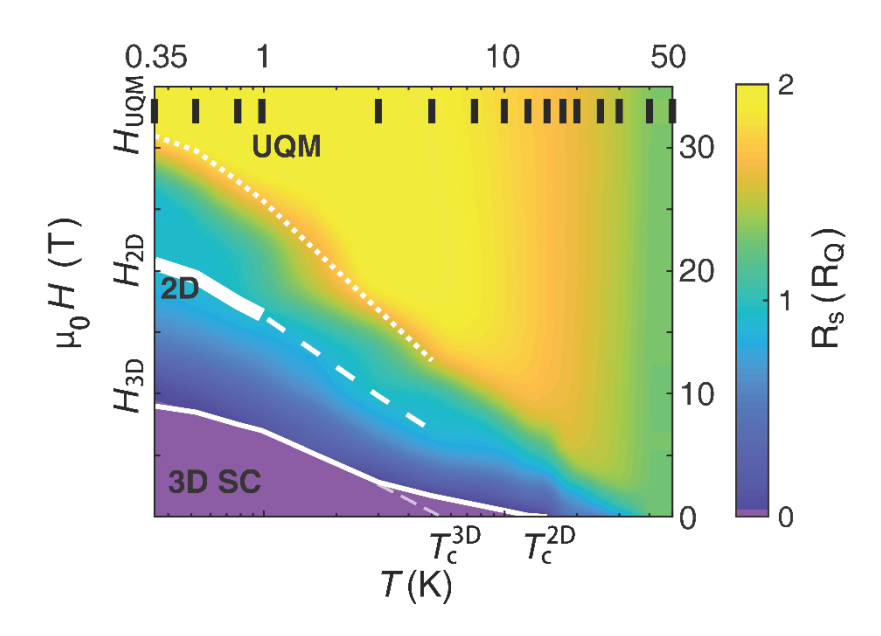


Fig. S1. Temperature-magnetic field phase diagram for A2.

Temperature-magnetic field phase diagram for A2 plotted with the identical method as that for A1 (Fig. 1A). Color map indicates the magnitude of R_s . Solid, dashed, and dotted white lines show H_{3D} , H_{2D} and H_{UQM} , respectively. Black bars at top indicate temperatures of measurements used to produce the phase diagram. A progression from 3D superconducting order, through a 2D order, to the ultra-quantum metal state is observed as a function of magnetic field. The characteristic fields H_{3D} , H_{2D} and H_{UQM} , are identical to those for A1. The phase diagram for A1 (Fig. 1A) and A2 (Fig. S1) are almost identical, except in the 2D SC regime. The broad white band indicates where $R_s \approx R_Q$ for A2, which is in the exact same region where 2D superconductivity is observed for A1 (Fig. 1A). $R_s \approx 2R_Q$ is observed in the ultra-quantum metal state for both A1 and A2. At higher temperatures, R_s for A1 and A2 lose quantization at $H = H_{2D}$ simultaneously.

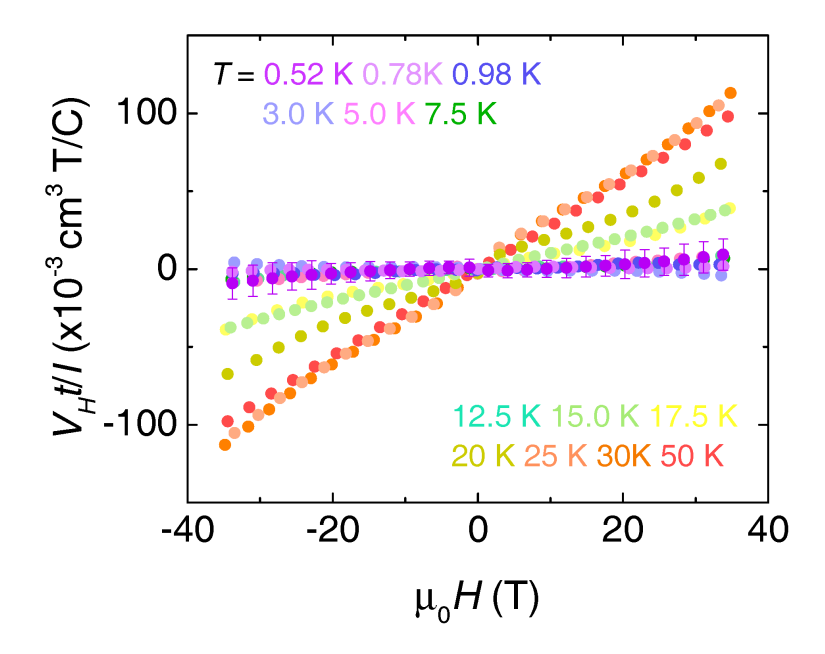


Fig. S2. Field-dependence of Hall voltage at various temperatures.

Hall voltage plotted as $V_H t/I$ versus magnetic field for all measured temperatures, where V_H is the Hall voltage, t is the sample thickness, and I is the current, respectively. Data are binned and antisymmetrized to remove the longitudinal magnetoresistance contribution that results from slight mis-alignment of voltage contacts. The nonlinear dependence on field comes from an imperfect cancellation of the longitudinal magnetoresistance contribution. Example of error bars due to noise are plotted for T = 0.52 K. Hall coefficient is obtained by a linear fit of the data for $|\mu_0 H| < 10$ T. The error bars shown in Fig. 1B come from the spread in values of R_H obtained over the entire field range, for a given temperature. Below 15 K, the Hall voltage is effectively zero. To put the magnitude of the low temperature response in perspective, consider the case of T = 0.52 K and field of 34 T; the value of R_H there is $2.8 \pm 3.0 \times 10^{-4}$ cm³/C. If we were to interpret this value as being due to fermionic quasiparticles, we would end up with a hole concentration of 2.1, which is not physically realistic. For comparison, the Hall coefficient for LBCO with x = 0.095 was measured previously in Ref. 17 for the same range of magnetic field. At low magnetic fields, our results for LBCO with x = 0.125 (Fig. 1B) are similar to those for LBCO with x = 0.095, but with a lower superconducting transition temperature.

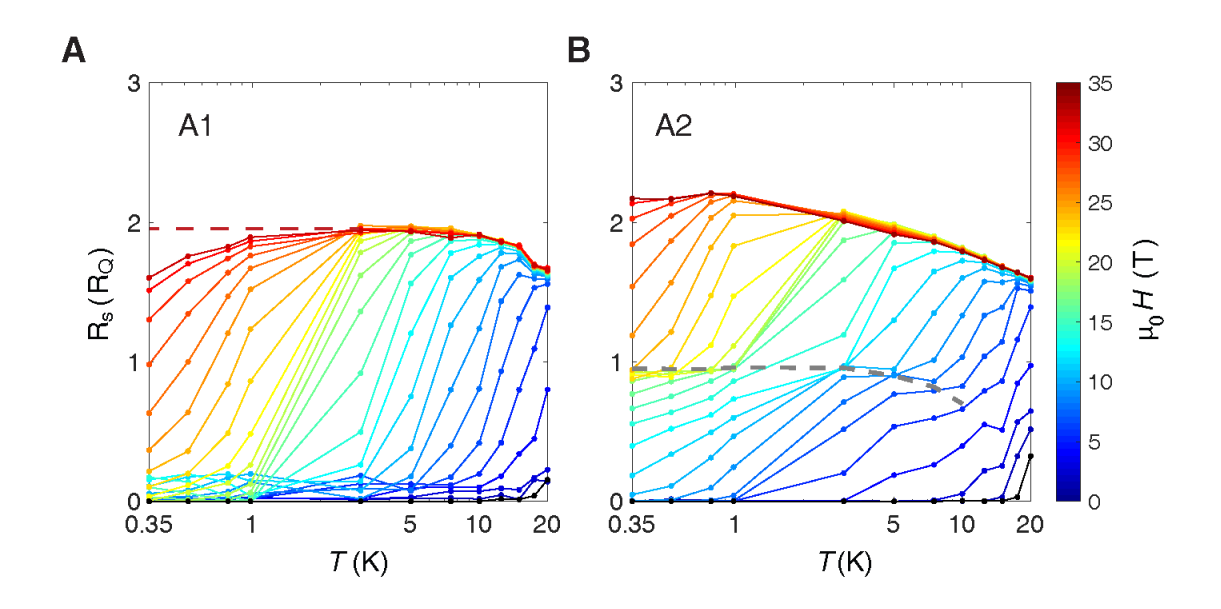


Fig. S3. Sheet resistance at constant magnetic field.

Sheet resistance of A1 (**A**) and A2 (**B**) vs. temperature at constant magnetic field, converted from data obtained by field sweeps, plotted in semi-log format. Color-coded solid lines indicate constant fields. The reentrant 2D superconductivity is visible in the figure for A1 and the corresponding quantization of $R_s \approx R_Q$ is indicated by a dashed grey band in the figure for A2. Dashed line for A1 indicates the saturation of resistivity at magnetic field slightly higher than 35 T, as obtained by extrapolating the scaling behavior apparent in Fig. 3D and E.

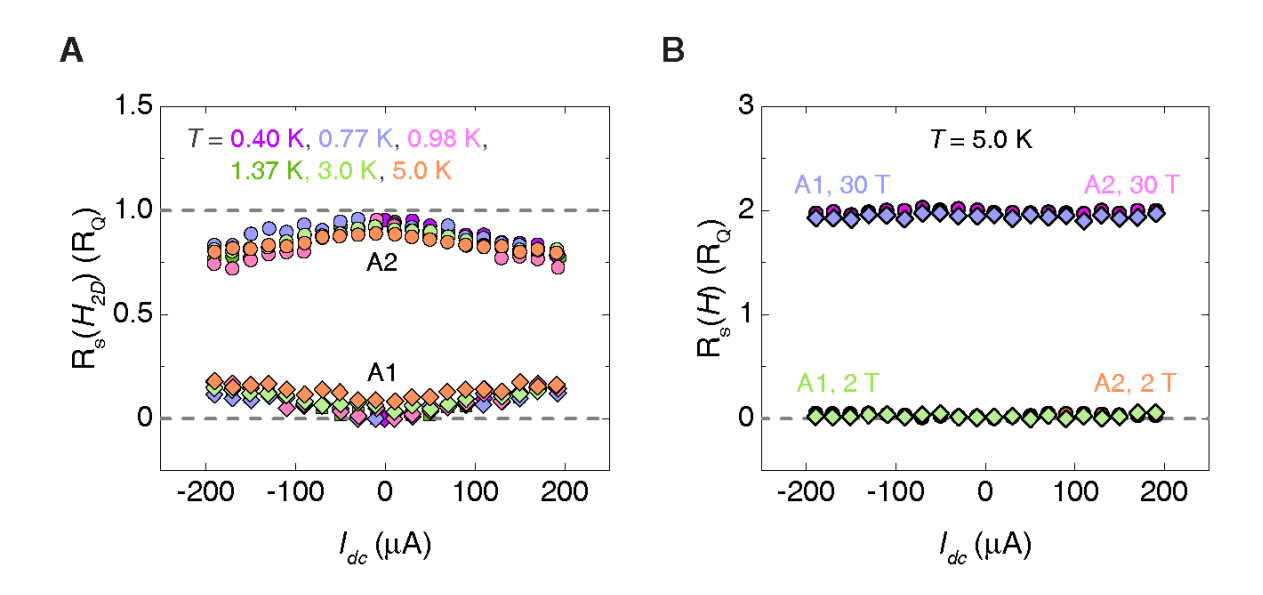


Fig. S4. ac nonlinear resistivity at H_{2D} for various temperatures.

(A) ac nonlinear resistivity at H_{2D} for all measured temperatures, $0.4 \le T \le 5$ K. The data at T = 0.98 K are included in Fig. 4C. R_s (H_{2D}) for A1 becomes non-zero at high dc current, while that for A2 deviates downwards from R_Q . At temperatures above 1 K, R_s (H_{2D}) for both A1 and A2 lose quantization even at lowest dc current (also shown in Fig. 4A, B). Data were taken at fields of 20 T, 17.5 T, 15 T, 13T, 9 T, and 6 T for T = 0.40 K, 0.77 K, 0.98 K, 1.37 K, 3.0 K, and 5.0 K, respectively. (B) ac resistivity at 2 T (below H_{3D}) and 30 T (above H_{UQM}) for T = 5 K. At both fields, ac resistivity is independent of the dc currents, in contrast to the nonlinear resistivity at H_{2D} in (A) and in Fig. 4C.

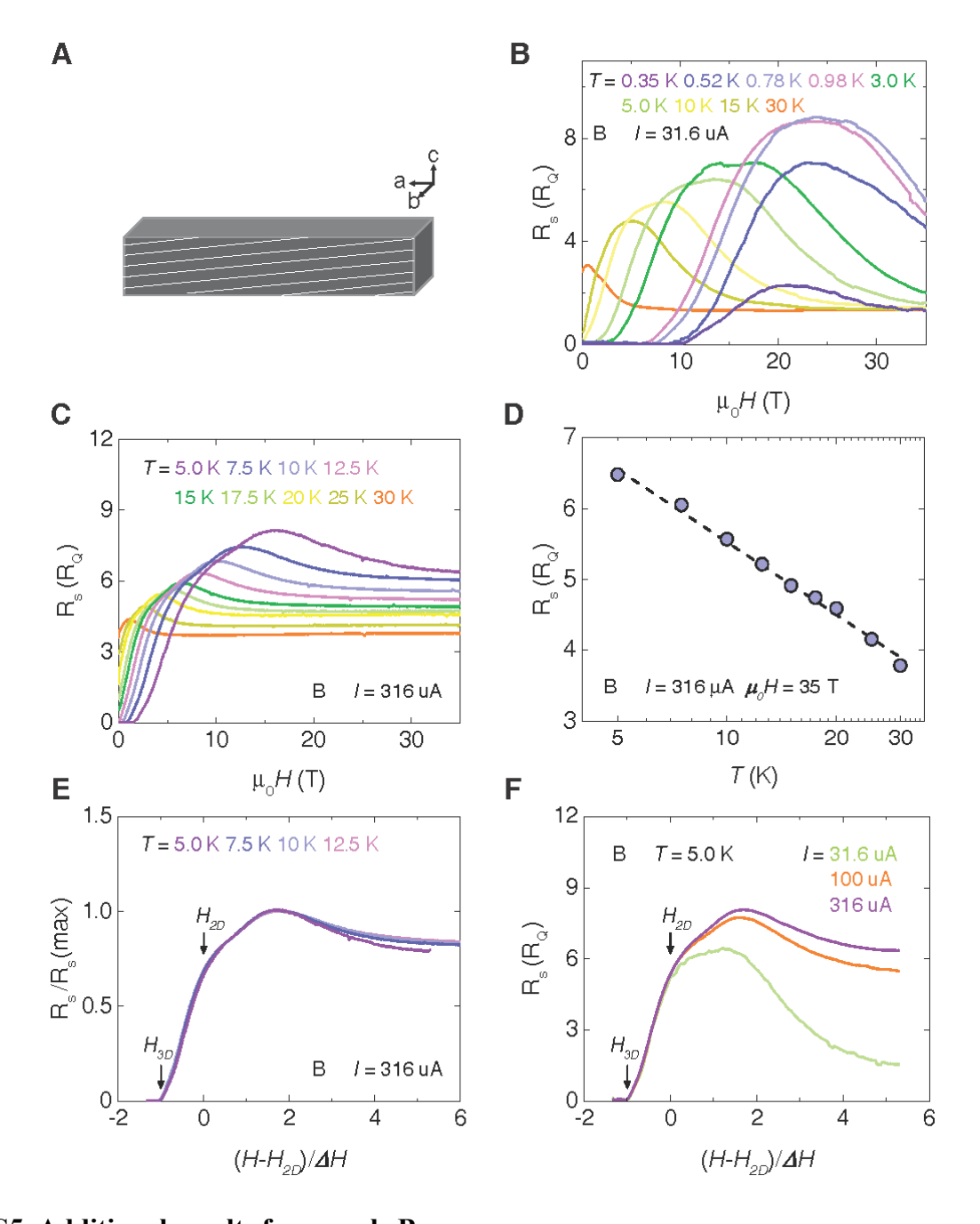


Fig. S5. Additional results for sample B. (A) Schematic illustration of *c*-axis misorientation for sample B; white lines indicate CuO_2 planes. (B) R_s at various temperatures with $I = 31.6 \mu A$. R_s at 0.35 K decreases to a magnitude

that is comparable to sample A1 and A2. (C) R_s at various temperatures with $I = 316 \,\mu\text{A}$, 10 times that shown in Fig. 3C. The R_s at high magnetic field and high current shows a non-metallic behavior, different from that at low current (Fig. 3C). (D) Semi-log plot of R_s at 15 T with $I = 316 \,\mu\text{A}$. The dashed line indicates the logarithmic temperature dependence. (E) Data same as in (C) but with the magnetic field scaled as in Fig. 3D-F. The magnitude of R_s is also normalized to the maximum value. The effect of temperature at high field is similar to that of the current. (F) R_s for various currents at T = 5 K. A dramatic difference of R_s is observed only for $H > H_{2D}$, in sharp contrast to the effect of current on A1 and A2 (Figs. 4 and S4).

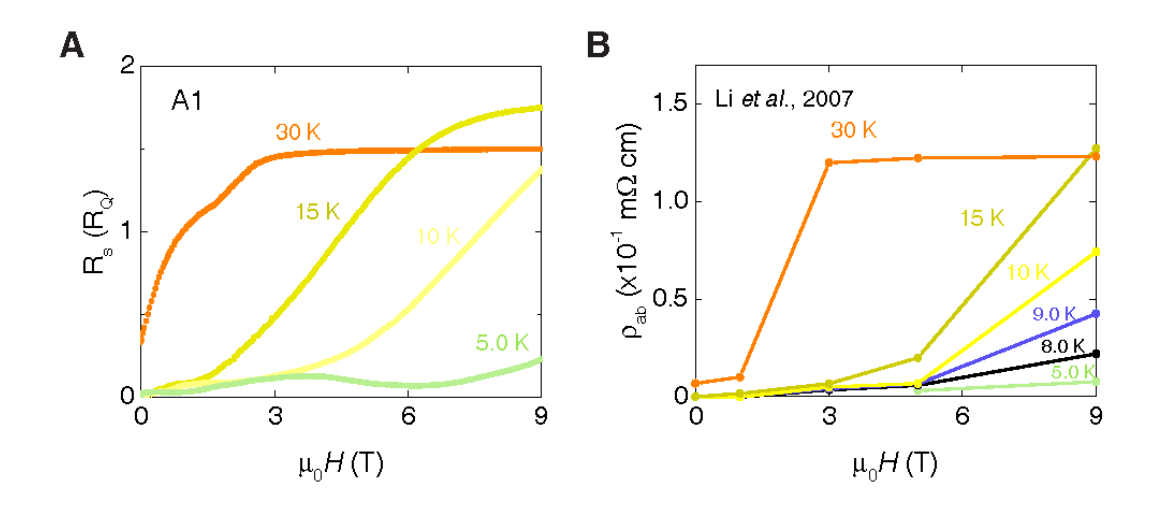


Fig. S6. Comparison between A1 and previous results for a similar sample.

(A) Sheet resistance as a function of magnetic field (below 9 T) of sample A1 for selected temperatures. The data for the full field range are included in Fig. 3A. R_s was measured with an ac current of 31.6 μ A. (B) In-plane resistivity vs. magnetic field previously reported for a related sample. The data at 0 T, 1 T, 3 T, 5 T, and 9 T are obtained from constant field measurements in Ref. 14 with a current much larger than 31.6 μ A. We note that, on converting to the same units, the resistivity magnitude is somewhat different for the two measurements, as it is sensitive to precise Ba and O concentrations and to measurements of the sample dimensions. Despite the differences between currents used and between data densities, an overall similarity is observed for the two samples.